Title

The hepatic compensatory response to elevated systemic sulfide promotes diabetes.

Authors

Roderick N. Carter[1], Matthew T.G. Gibbins[1,a], Martin E. Barrios-Llerena[1,b], Stephen E. Wilkie[1,2], Peter L. Freddolino[3], Marouane Libiad[3,c], Victor Vitvitsky[3], Barry Emerson[1,d], Thierry Le Bihan[4,e], Madara Brice[1], Huizhong Su[5,f], Scott G. Denham[1], Natalie Z.M. Homer[1], Clare Mc Fadden[1,g], Anne Tailleux[6], Nourdine Faresse[7,h], Thierry Sulpice[7], Francois Briand[7], Tom Gillingwater[8], Kyo Han Ahn[9], Subhankar Singha[9,i], Claire McMaster[10], Richard C. Hartley[10], Bart Staels[6], Gillian A. Gray[1], Andrew J. Finch[5,j], Colin Selman[2], Ruma Banerjee[3], Nicholas M. Morton[1*]

[1]University/British Heart Foundation Centre for Cardiovascular Science, University of Edinburgh, Queen's Medical Research Institute, Edinburgh, EH16 4TJ, United Kingdom

[2]Glasgow Ageing Research Network (GARNER), Institute of Biodiversity, Animal Health and Comparative Medicine, University of Glasgow, Glasgow, G12 8QQ, United Kingdom

[3]The Department of Biological Chemistry, University of Michigan Medical School, Ann Arbor, MI 48109, USA

[4]SynthSys - Systems and Synthethic Biology, Edinburgh, EH9 3JD, United Kingdom

[5]Cancer Research UK Edinburgh Centre, MRC Intitute of Genetics & Molecular Medicine, University of Edinburgh, Western General Hospital, Edinburgh, EH4 2XR, United Kingdom

[6]Université de Lille, Inserm, CHU Lille, Institut Pasteur de Lille, U101-EGID, F-59000, Lille, France

[7]Physiogenex S.A.S, Prologue Biotech, 516 rue Pierre et Marie Curie, 31670 Labège, France

[8]College of Medicine & Veterinary Medicine, University of Edinburgh, Old Medical School (Anatomy), Teviot Place, Edinburgh, EH8 9AG, United Kingdom

[9]Department of Chemistry, POSTECH, 77 Cheongam-Ro, Nam-Gu, Pohang, Gyungbuk, 37673, South Korea

[10]School of Chemistry, Joseph Black Building, University of Glasgow, Glasgow, G12 8QQ, United Kingdom

Current affiliations where different from the place where work for the manuscript was carried out;

[a]Cambridge Biomedical Campus, Royal Papworth Hospital NHS Foundation Trust, Cardiology department, Cambridge, CB2 0AY, United Kingdom

[b]The International Clinical Research Centre, St. Anne's University Hospital, Brno, 656 91, Czech Republic

[c]Institute for Integrative Biology of the Cell (I2BC), CEA, CNRS, Univ. Paris-Sud, Université Paris-Saclay, 91198, Gif-sur-Yvette cedex, France

[d]BD Research Centre Ireland, Co. Limerick, Castletroy, Ireland

[e]Rapid Novor Inc, 44 Gaukel St, Kitchener, ON N2G 4P3, Canada

[f]Wellcome Trust Centre for Mitochondrial Research, Newcastle University, NE2 4HH, United Kingdom

[g]Springer Nature Campus, London, N1 9FN, United Kingdom

[h]D.I.V.A-expertise, 1 place Pierre Potier, 31100 Toulouse, France

[i]Institute of Advanced Studies and Research, JIS University, Kolkata 700091, India

[j]Cancer Research UK Barts Centre, London, EC1M 6BQ, United Kingdom

[*]**Lead Contact details:** Nicholas M. Morton

Molecular Metabolism Group, University/British Heart Foundation Centre for Cardiovascular Science, University of Edinburgh, Queen's Medical Research Institute, Edinburgh, EH16 4TJ, United Kingdom.

nik.morton@ed.ac.uk

Conflict of interests statement

The authors have declared that no conflict of interest exists.

Abstract

Impaired hepatic glucose and lipid metabolism are hallmarks of type–2 diabetes. Increased sulfide production from cysteine, or sulfide–donor compounds, may beneficially regulate hepatic metabolism. Disposal of sulfide through the sulfide oxidation pathway (SOP) is critical for maintaining sulfide within a safe physiological range. We show that mice lacking the liver–enriched mitochondrial SOP enzyme thiosulfate sulfur–transferase (*Tst*$^{-/-}$ mice) exhibit high circulating sulfide, increased gluconeogenesis, hypertriglyceridemia and fatty liver, despite whole–body insulin–sensitisation. Unexpectedly, hepatic sulfide levels were normal in *Tst*$^{-/-}$ mice, a result of homeostatic induction of mitochondrial sulfide disposal and glutathione excretion associated with net suppression of protein persulfidation and nuclear respiratory factor–2 target proteins. Proteomic and persulfidomic profiling converged on gluconeogenesis and hepatic lipid metabolism and revealed a selective deficit in medium–chain fatty acid oxidation in *Tst*$^{-/-}$ mice. We reveal a critical role for TST in hepatic metabolism that raises implications for sulfide-donor strategies in the context of liver function and metabolic disease.

67 # Introduction

68 The prevalence of Type 2 diabetes (T2D) continues to soar in parallel with that of obesity[1].
69 Increased hepatic glucose production and aberrant hepatic lipid metabolism are cardinal
70 features of T2D[2,3]. Dysregulation of hepatic nutrient metabolism in T2D is a promising area
71 for therapeutic intervention because it precipitates the more severe liver pathologies that
72 manifest along the spectrum of non-alcoholic fatty liver disease (NAFLD), steatosis,
73 steatohepatitis and hepatocellular carcinoma[4].

74 Hydrogen sulfide (hereafter referred to as sulfide), an endogenously produced gaseous
75 signalling molecule[5–8], has recently emerged as a modulator of nutrient metabolism[9–12].
76 Enzymatic sulfide production from sulfur amino acids is catalysed by cystathionine beta–
77 synthase; CBS, and cystathionine gamma lyase; CTH[13,14] and by 3-mercaptopyruvate sulfur
78 transferase; MPST[15–17]. Thioredoxin-mediated reduction of cysteine persulfides on proteins
79 also regulates free sulfide and cysteine persulfide levels[18]. Endogenously produced and
80 exogenously administered sulfide specifically influences hepatic glucose and lipid
81 metabolism[19,20]. Thus, *in vitro,* treatment of murine hepatocytes with NaHS, or
82 overexpression of rat *Cth* in HepG2 liver cells, increased glucose production through increased
83 gluconeogenesis and reduced glycogen storage[21]. Conversely, glucose production was lower
84 in hepatocytes from *Cth* gene knockout mice ($Cth^{-/-}$ mice) that exhibit low sulfide
85 production[21]. Elevation of sulfide with NaHS administration *in vivo* reduced cholesterol and
86 triglyceride accumulation in the liver of high fat diet (HFD)–fed mice[22]. In contrast, inter-cross
87 of sulfide production–deficient $Cth^{-/-}$ mice with the hyperlipidemic $Apoe^{-/-}$ mouse strain
88 ($Cth^{-/-}Apoe^{-/-}$ mice) produced a phenotype of elevated plasma cholesterol following
89 exposure to an atherogenic diet[23]. Consistent with their higher cholesterol, $Cth^{-/-}Apoe^{-/-}$
90 mice developed fatty streak lesions earlier than $Apoe^{-/-}$ mice, and this effect was reversed

91 by NaHS administration[23]. Sulfide may also indirectly impact hepatic nutrient metabolism
92 through its effect on hepatic artery vasorelaxation and thus liver perfusion[24,25]. The
93 apparently beneficial effects of sulfide administration in multiple disease indications has led
94 to a major drive towards development of targeted H_2S–donor molecules as a therapeutic
95 approach[26,27]. However, an often-overlooked aspect of net sulfide exposure, key to the
96 efficacy of therapeutic H_2S–donors, is that it is regulated through its oxidative disposal. Thus,
97 endogenous sulfide exposure is actively limited to prevent mitochondrial respiratory
98 toxicity[28–30]. Sulfide is rapidly oxidized[31,32] through the mitochondrial sulfide oxidation
99 pathway (SOP), consisting of sulfide quinone oxidoreductase (SQOR), persulfide dioxygenase
100 (ETHE1/PDO) and thiosulfate sulfurtransferase (TST, also known as rhodanese)[31,33,34]. The
101 liver is highly abundant in SOP enzymes, and is a major organ of whole body sulfide disposal[32].
102 Mice lacking the *Ethe1* gene (*Ethe1*$^{-/-}$ mice) die of fatal sulfide toxicity[30], consistent with its
103 critical role in sulfide oxidation and the severe pathological consequences of unchecked
104 sulfide build-up in tissues. However, the importance of mitochondrial TST in the SOP *in vivo*
105 remains obscure. In contrast to *Ethe1*$^{-/-}$ mice, *Tst*$^{-/-}$ mice were grossly normal despite
106 exhibiting substantially elevated blood sulfide levels, as implied by qualitative measures[35].
107 This revealed an important yet distinct role for TST in the SOP for the first time *in vivo*.
108 Nevertheless, *Tst*$^{-/-}$ mice showed an apparently diabetogenic impairment of glucose
109 tolerance[35], consistent with the concept that increased sulfide promotes hepatic glucose
110 production[21]. As *Tst* deficiency represents a model of chronic but viable sulfide elevation,
111 determining the molecular mechanisms driving their aberrant metabolic profile can provide
112 important insights into the optimal range for therapeutic sulfide exposure, particularly in light
113 of the current interest in developing mitochondrially–targeted sulfide–donors[36,37]. To this end

114 we sought to define the impact of *Tst* deficiency on the underlying molecular pathways that

115 impact hepatic metabolism.

116

117 # Results

118 *Tst$^{-/-}$ mice exhibit increased hepatic gluconeogenesis and dyslipidaemia despite mild*
119 *peripheral insulin sensitisation.*

120 TST *mRNA* expression is highest in the liver (e.g. it is ~8-fold higher than in white adipose
121 tissue http://biogps.org/#goto=genereport&id=22117). We therefore hypothesised that liver
122 TST deficiency was the principal driver of the impaired glucose tolerance previously observed
123 in *Tst*$^{-/-}$ mice[35]. *Tst*$^{-/-}$ mice exhibited higher glucose levels than C57BL/6J controls in
124 response to a pyruvate challenge, consistent with higher hepatic glucose production (Figure
125 1A). We next tested phosphoenolpyruvate carboxykinase (PEPCK) activity, a key enzyme of
126 *de-novo* hepatic glucose synthesis, and found it was higher in liver homogenates from *Tst*$^{-/-}$
127 mice (Figure 1B). Next, we performed a 1 hour $^{13}C_3$-pyruvate metabolite–pulse incorporation
128 experiment in isolated hepatocytes cultured in $^{12}C_3$-pyruvate–free medium. Hepatocytes
129 from *Tst*$^{-/-}$ mice displayed ^{13}C labelling consistent with increased metabolism of pyruvate to
130 oxaloacetate – a critical early step in gluconeogenesis. Specifically, aspartate, which is derived
131 from pyruvate via oxaloacetate was significantly increased in the *Tst*$^{-/-}$ (Figure 1C). A trend
132 towards higher $^{13}C_3$ malate, and lower $^{13}C_2$ acetyl–CoA was also observed (Figure S1A and
133 S1B). $^{13}C_3$ Lactate was similar between genotypes, suggesting a similar activity of glycolytic
134 disposal of pyruvate through lactate dehydrogenase (Figure S1A and S1B). Total pool sizes for
135 all measured metabolites were similar between genotypes (Figure S1C). Consistent with
136 increased endogenous glucose production in the *Tst*$^{-/-}$ mice, fasting plasma glucose was
137 higher in *Tst*$^{-/-}$ mice relative to 6J mice during the pre-clamp 3-^{3}H glucose tracer infusion
138 phase (60-90 minutes post tracer) of euglycemic, hyperinsulinemic (EH) clamp experiments
139 (Figure 1D, Table S1A). Higher plasma glucose levels in *Tst*$^{-/-}$ mice under these conditions

140 was not explained by lower glucose utilization in *Tst*$^{-/-}$ mice; glycogen synthesis and
141 glycolysis were comparable between genotypes across 60–90 minutes (Table S1A). Glucose
142 turnover – a derived parameter used to infer glucose production – was also comparable
143 between genotypes (Table S1A). However, derivation of glucose turnover requires that
144 glucose levels are stable during the period in which it is calculated. In our pre-clamp baseline
145 period, a highly significant effect of time (Figure 1D) indicated that this assumption was not
146 met, and thus true endogenous glucose production cannot be inferred from the glucose
147 turnover parameter in this instance. Combined with the pyruvate tolerance, PEPCK activity
148 and $^{13}C_3$-pyruvate pulse data, higher fasting glucose levels in the *Tst*$^{-/-}$ mice, given
149 comparable glucose utilization, is most likely due to higher endogenous glucose production
150 in the *Tst*$^{-/-}$ mice.

151 We next wished to explore whether the changes to glucose metabolism were driven by insulin
152 resistance. Liver glycogen, a marker of long–term carbohydrate storage typically impaired
153 with insulin resistance, was comparable between *Tst*$^{-/-}$ and C57BL/6J control mice (Figure
154 S2A). Despite unchanged steady–state markers of hepatic insulin sensitivity, impaired glucose
155 tolerance, previously described in the *Tst*$^{-/-}$ mice[35], suggested that whole body, and usually
156 hepatic, insulin–resistance was present. We investigated this using the euglycaemic clamp
157 where, unexpectedly, we observed whole–body insulin sensitisation under these short–term
158 steady–state conditions. During the clamp, when insulin was high, and blood glucose levels
159 were maintained constant, the glucose infusion rate was comparable between genotypes
160 (Table S1B). However, an increase in whole–body glucose uptake (integral glucose) by tissues
161 in the *Tst*$^{-/-}$ mice was apparent (Figure 1E, Table S1B), supporting increased peripheral
162 insulin–sensitivity, with a directionally consistent trend for increased glucose uptake into
163 several tissues. We confirmed this finding using standard insulin tolerance tests, where the

164 glucose decrement in response to insulin was greater in *Tst*$^{-/-}$ mice (Figure 1F, Figure S2B).
165 Together these data demonstrate a net increase in dynamic whole–body insulin sensitivity,
166 despite increased hepatic glucose output in *Tst*$^{-/-}$ mice. Finally, we assessed whole–body
167 glucose homeostasis with the EH–clamp method after chronic HFD feeding. Under these
168 conditions, *Tst*$^{-/-}$ mice maintained increased heptic glucose output (Figure 1D) but showed
169 convergence of the insulin–sensitivity profile to that of the C57BL/6J mice.
170 We also assessed whether *Tst* deficiency was associated with impaired lipid metabolism,
171 another hallmark of diabetes. Fast protein liquid chromatography analysis of triglyceride
172 levels and their lipoprotein distribution revealed significantly higher total plasma triglycerides
173 in *Tst*$^{-/-}$ mice (Figure 1G). The higher triglyceride was selectively associated with an
174 increased VLDL triglyceride fraction (Figure 1G), consistent with a dominant liver-driven
175 impairment in lipid metabolism[38]. Total and distinct lipoprotein fraction plasma cholesterol
176 levels were similar between genotypes (Figure S2C and S2D), suggestive of a triglyceride–
177 selective effect of *Tst* deficiency on hepatic lipid efflux. HFD significantly increased liver lipid
178 content of C57BL/6J mice but did not further increase the elevated lipid levels in the liver of
179 *Tst*$^{-/-}$ mice (Figure 1H-1I).

180 *TST deficiency elicits compensatory hepatic sulfide disposal mechanisms that drive reduced*
181 *global protein persulfidation.*

182 A role for TST in the disposal of sulfide was suggested by its participation in the SOP[31,34] and
183 supported *in vivo* by the qualitatively higher blood sulfide of *Tst*$^{-/-}$ mice[35]. Here, we
184 quantified circulating sulfide, showing approximately 10–fold elevation in the blood and
185 plasma of *Tst*$^{-/-}$ mice (Table 1A and 1B). Thiosulfate, an oxidised metabolite of sulfide [39,40]
186 and a TST substrate[41], was approximately 20–fold higher in plasma (Table 1B), and profoundly

187 higher (450–fold) in urine (Table 1C) of *Tst*$^{-/-}$ mice compared to C57Bl/6J mice. Reduced
188 glutathione (GSH) levels were ~2–fold higher in the plasma of *Tst*$^{-/-}$ mice (Table 1B). To
189 determine any direct hepatic contribution to the elevated systemic sulfide *in vivo*, whole
190 blood was sampled from the inferior vena cava (IVC) (Table 1D). IVC sulfide levels tended to
191 be higher in the *Tst*$^{-/-}$ mice, but the magnitude of the increase (~3-fold) did not parallel that
192 in trunk blood (~10-fold), suggesting liver was not a major source of the elevated circulating
193 sulfide. Surprisingly, liver homogenate sulfide, thiosulfate, cysteine and GSH levels were
194 similar between *Tst*$^{-/-}$ and C57BL/6J mice (Table 1E). Further, cultured hepatocytes from
195 *Tst*$^{-/-}$ and C57BL/6J mice exhibited similar intracellular sulfide levels, as estimated using P3,
196 a sulfide–selective fluorescent probe[42] (Table 1F). Mitochondrial sulfide levels in liver
197 reported by MitoA/MitoN[43] were similarly unchanged between genotypes (Table 1G). The
198 apparently unaltered hepatic steady-state sulfide levels, despite higher circulating sulfide,
199 suggested a profound homeostatic mechanism was invoked in the liver of *Tst*$^{-/-}$ mice. We
200 assessed respiratory sulfide disposal (antimycin–sensitive) and found this was markedly
201 increased in hepatocytes from *Tst*$^{-/-}$ mice, whereas antimycin–insensitive sulfide disposal
202 was relatively reduced compared to hepatocytes from C57BL/6J mice (Table S2). Isolated liver
203 mitochondria from *Tst*$^{-/-}$ hepatocytes also exhibited a higher sulfide disposal rate (Table S2).
204 In addition, cysteine and GSH was excreted at higher levels from *Tst*$^{-/-}$ hepatocytes under
205 basal conditions and after stimulation of sulfur amino acid metabolism by addition of
206 methionine (Figure 2A and 2B). Consistent with higher GSH turnover, hepatocytes from *Tst*$^{-}$
207 $^{/-}$ mice showed resistance to exogenous H_2O_2–mediated mitochondrial ROS production
208 (Figure S3). We next determined the global hepatic protein persulfidation profile, the major
209 post–translational modification mediated by sulfide[44–46]. Mass spectrometry analysis of
210 maleimide–labelled liver peptides revealed a greater abundance of peptides with a lower

211 persulfidation level (under-persulfidated) in the liver of *Tst*$^{-/-}$ mice (Figure 2C). We
212 confirmed this using semi-quantitative western–blot analysis on pulled down maleimide–
213 labelled proteins (Figure 2D). Gene Ontology (GO) analysis of proteins exhibiting altered
214 persulfidation levels revealed 28 terms different between *Tst*$^{-/-}$ and C57BL/6J mice by log–
215 fold change (Table 2). Major under-persulfidated terms (20) included "*FAD-binding*, *methyl*
216 *transferase, peroxisome, acyl-CoA dehydrogenase activity and transaminase*" while the less
217 abundant over-persulfidated terms (8) were dominated by terms related to "*Nicotinamide*
218 *metabolism*". Given evidence for altered gluconeogenesis above, we also performed a
219 pathway specifc analysis of the persulifidome. Persulfidation of proteins involved in
220 gluconeogenesis showed a mixture of under and over–persulfidated cysteines with a strong
221 enrichment of over-persulfidation , a pattern that was significantly different from the overall
222 persulfidation profile of the liver from *Tst*$^{-/-}$ mice (Figure S4A). We further found that the
223 gluconeogenesis pathway also exhibited a significantly higher magnitude of change
224 (independent of direction of change) in persulfidation than in the overall profile of the liver
225 of *Tst*$^{-/-}$ mice (Figure S4B).

226 *The hepatic proteome of Tst*$^{-/-}$ *mice reveals a distinct molecular signature of altered sulfur*
227 *and mitochondrial nutrient metabolism.*

228 To gain molecular insight into the mechanisms underlying the apparently diabetogenic liver
229 phenotype in ND-fed *Tst*$^{-/-}$ mice, we performed a comparative iTRAQ proteomic analysis of
230 whole liver with ND-fed C57BL/6J mice. Kyoto Encyclopedia of Genes and Genomes (KEGG)
231 analysis (at significance threshold $P < 0.05$) revealed 4 up–regulated pathways in liver of *Tst*$^{-}$
232 $^{/-}$ mice related to amino acid metabolism, including sulfur amino acids, and sulfur metabolism
233 (Table 3A). GO analysis (at threshold $P < 0.05$) revealed 95 significantly up–regulated terms in

234 liver of *Tst*$^{-/-}$ mice (Table S3A). Of the top 14 up–regulated terms, 7 referred to amino acid
235 metabolism and 1 referred to the organellar term '*mitochondrion*'. KEGG pathway analysis
236 revealed 27 down–regulated pathways in the liver of *Tst*$^{-/-}$ mice (Table 3B) including Phase
237 1 and 2 detoxification pathways (Cytochrome P450s, Glutathione and Glucuronidation) and
238 '*Lysosome*', '*Protein processing in the Endoplasmic reticulum'* organellar terms. 213 GO terms
239 were significantly down–regulated in *Tst*$^{-/-}$ mice (Table S4B). Among the most significant
240 down–regulated terms were phase 2 detoxification pathways such as *'glutathione binding'*
241 and '*glutathione transferase activity'* and '*endoplasmic reticulum'*. We validated a
242 representative subset of protein changes (Figures S5A and S5D), noting broadly consistent
243 direction of change in the key pathways. At the single protein level, the most robust change
244 we observed was increased MPST protein in whole liver (Figure S5A and S5D) and
245 mitochondrial sub-fractions (Figure S5B and S5D). This change was remarkable as mRNA levels
246 for *Mpst* were lower in *Tst*$^{-/-}$ mice (Figure S5C), likely as a result of loss of proximal *Mpst*
247 promoter function; *Mpst* is a paralog of *Tst*[47] juxtaposed approximately 1kb from the *Tst* gene.
248 Protein levels for other sulfide producing and disposal enzymes were comparable between
249 genotypes (Table S4). Given the evidence for glucose and lipid metabolic changes in the *Tst*$^{-}$
250 $^{/-}$ mice, we undertook a further focussed comparison of canonical proteins in these pathways
251 (Table S5). Four GO terms were enriched in liver from *Tst*$^{-/-}$ mice, all of which were down–
252 regulated; '*Lipid metabolic process'*, *'fatty acid beta-oxidation'*, *'Acyl-CoA dehydrogenase*
253 *activity' and 'Acyl-CoA hydrolase activity'* (Table S5). Notably, supportive of largely unchanged
254 hepatic insulin sensitivity, canonical insulin–regulated proteins[48, 49] were expressed
255 comparably between genotypes (Tables S6 and S7).

256 *Hepatic protein expression in Tst*$^{-/-}$ *mice is consistent with lower NRF2 activation*.

257 We performed a transcription factor binding site (TFBS) enrichment analysis in the promoters
258 of proteins that are up–regulated in the liver of *Tst*$^{-/-}$ mice to look for potential hub
259 transcriptional drivers of the proteome profile (Figure S6A). This revealed a statistically
260 significant under-representation of TFBS for the sulfide–responsive[50,51] NRF2 transcription
261 factor (Figure S6A). To explore whether there was evidence for reduced NRF2 activation in
262 the *Tst*$^{-/-}$ liver, we looked at the relative expression of 47 NRF2–regulated proteins in the
263 proteome of ND-fed *Tst*$^{-/-}$ and ND-fed C57Bl/6J mice. While 37 of these target proteins were
264 similar in expression between the genotypes, 10 NRF2 target proteins were lower in the liver
265 of *Tst*$^{-/-}$ mice (Figure S6B) and none of the 47 NRF2 target proteins were increased in *Tst*$^{-/-}$
266 liver.

267 *Proteome of TST deficiency versus HFD response in C57BL/6J mice reveals distinct regulation*
268 *of lipid metabolism, sulfide metabolism and detoxification pathways.*

269 We examined mechanistic commonalities between the diabetogenic hepatic phenotype of
270 *Tst*$^{-/-}$ mice and that induced by the diabetogenic HFD–feeding regimen in C57BL/6J mice.
271 Note, ND-fed *Tst*$^{-/-}$ mice were in a pre-existing diabetogenic state (Figure 1) that does not
272 further worsen with HFD (Figure 1H-I, Table S1), suggesting gross phenotypic convergence of
273 the two genotypes after HFD. We compared the identity and direction of change of the 188
274 proteins differentially expressed in ND-fed *Tst*$^{-/-}$ mice (versus ND-fed C57BL/6J mice; Figure
275 3A) to proteins that were differentially expressed in response to HFD in C57BL/6J mice (432
276 proteins; Figure 3A). There was a striking 67% overlap in individual proteins (126) in this
277 comparison (Figure 3A). When we analysed these two protein signatures for directionally
278 shared pathways, one up-regulated KEGG pathway *'Glycine, serine and threonine metabolism'*
279 (Table S8A) and 12 down-regulated KEGG pathways, including *'drug metabolism'* and

280 *'endoplasmic reticulum'* (Table S8B) were common to the liver of the ND-fed *Tst*$^{-/-}$ and HFD-
281 fed C57BL/6J mice. Consistent with a pre-existing HFD–like proteome, the dynamic response
282 to HFD in the liver of *Tst*$^{-/-}$ mice was muted, relative to that observed in C57BL6J mice (106
283 proteins, a 4–fold lower response; Figure 3B). Focussing on the sulfide pathway, MPST and
284 SUOX were increased by HFD in 6J and *Tst*$^{-/-}$ mice (Table S9). The HFD–induced increase in
285 MPST was less pronounced in the liver of *Tst*$^{-/-}$ mice, likely a reflection that it is already
286 elevated in ND–fed *Tst*$^{-/-}$ mice. We then considered contrasting, rather than congruent,
287 proteomic responses arising from TST deficiency versus HFD responses in C57BL/6J mice to
288 illuminate potential novel pathways underlying the otherwise functionally similar
289 diabetogenic hepatic *Tst*$^{-/-}$ phenotype. 5 KEGG pathways (Table S10A) and 4 GO terms (Table
290 S10B) were regulated in the opposite direction in this comparison. Strikingly, the GO terms
291 were all related to lipid metabolism, which were up–regulated in the HFD response but down–
292 regulated with TST deficiency (Table S10A-B). An organelle–focussed protein analysis showed
293 shared up-regulation of mitochondrial and endoplasmic reticulum pathways between TST
294 deficiency (Figure 3C upper row) and C57BL/6J HFD-responses (Figure 3C lower row), but a
295 striking discordance in peroxisomal protein pathways (up-regulated by HFD, down-regulated
296 TST deficiency) and nuclear proteins (down-regulated by HFD, up-regulated TST deficiency;
297 Figure 3C).

298 *The Tst*$^{-/-}$ *liver proteome and persulfidome converge on transamination and lipid oxidation*
299 *pathways.*

300 To assess whether conservation of changes at protein and post-translational modification
301 levels can illuminate key regulatory hubs driving the hepatic phenotype we ran a congruence
302 analysis of the proteome and persulfidome. We found that GO terms referring to *amino acid*,

303 *lipid metabolism* and *peroxisome* were significantly regulated at both the level of protein
304 abundance and persulfidation status (Table 4).

305 *Tst*$^{-/-}$ *hepatocytes exhibit elevated mitochondrial respiration and a defect in medium–chain*
306 *fatty acid oxidation.*

307 Enhanced respiratory sulfide disposal was found from *Tst*$^{-/-}$ hepatocytes, and enrichment of
308 mitochondrial proteins was suggested from the liver proteome of the *Tst*$^{-/-}$ mice (Table S4).
309 We therefore sought to determine if TST deficiency affected respiratory function and
310 substrate utilisation of the hepatocyte. Analysis of electron micrographs prepared from the
311 liver of ND-fed *Tst*$^{-/-}$ mice and C57BL/6J controls showed morphologically normal
312 mitochondria (Figure 4A). Basal respiration, comprising ATP–linked and leak respiration, was
313 significantly higher in hepatocytes from *Tst*$^{-/-}$ mice (Figure 4B–4D). Maximal hepatocyte
314 respiratory capacity and non–respiratory oxygen consumption was similar between
315 genotypes (Figures S7A and S7B). In line with phenotypic convergence following HFD,
316 hepatocyte respiration was comparable between genotypes from HFD-fed mice (Figures S7C-
317 S7H). A unique feature of the liver from *Tst*$^{-/-}$ mice that contrasted with HFD response in
318 C57BL/6J mice was a decrease in proteins and persulfidation levels of proteins in lipid
319 oxidation pathways. We therefore investigated hepatocyte respiration of lipids. Using a low
320 pyruvate (100 μM) medium to reveal respiratory dependency on other substrates, we showed
321 that CPT1A–mediated mitochondrial oxidation of endogenous long chain fatty acids (LCFA;
322 etomoxir-inhibited) was similar between genotypes (Figure 4E). Next, we by–passed CPT1A–
323 mediated LCFA transfer, and revealed a marked deficit in respiration stimulated by the
324 medium chain fatty acid octanoate in hepatocytes from *Tst*$^{-/-}$ mice (Figure 4F). A similar
325 experiment adding back pyruvate revealed comparable stimulation of respiration between

326 genotypes (Figure S6I). In amino acid free media, combined glutamine–, aspartate– and
327 alanine–stimulated hepatocyte respiration was comparable between genotypes (Figure S6J).
328

329 # Discussion

330 Elevated TST expression in adipose tissue was recently identified as a genetic mechanism
331 driving metabolically protective leanness in mice[35]. Conversely, mice with genetic deletion of
332 *Tst* (*Tst*$^{-/-}$ mice) exhibited impaired glucose tolerance relative to C57BL/6N controls[35]. A key
333 observation from the *Tst*$^{-/-}$ mouse was qualitative evidence for elevated blood sulfide
334 levels[35], which implicated the mitochondrial sulfurtransferase as playing an important role in
335 the sulfide oxidation pathway (Figure S8) for the first time *in vivo*. However, the mechanistic
336 link between *Tst* deficiency and impaired glucose tolerance remained unclear. The *Tst*$^{-/-}$
337 mice had a subtle adipose tissue phenotype, with comparable fat accumulation upon high fat
338 feeding, suggesting alternate organs as a potential source of impaired glucose homeostasis.
339 Moreover, TST is most highly abundant in the liver, consistent with its role in detoxification
340 of cyanide and related molecules. Indeed, hepatic TST mRNA levels are ~8-fold higher than
341 adipose tissue, with the difference in enzyme activity likely substantially exceeding this, per
342 gram of tissue. Based upon the reported effects of sulfide to increase hepatic glucose
343 production[20,21] and modulate lipid metabolism[22,23], we hypothesised that TST deficiency
344 predominantly drives a diabetogenic state through increased hepatic sulfide exposure.
345 Consistent with this, we found evidence supportive of increased gluconeogenesis, steatosis,
346 elevated plasma VLDL triglycerides and, quantitatively, a 10-fold higher circulating blood
347 sulfide level in *Tst*$^{-/-}$ mice. Unexpectedly, and in spite of the markedly increased circulating
348 sulfide levels, steady-state sulfide level was normal in the liver of *Tst*$^{-/-}$ mice. Moreover, we
349 found evidence for multiple mechanisms for increased, not decreased, hepatic sulfide
350 disposal, reduced downstream sulfide signalling and novel molecular explanations for the
351 apparently diabetogenic phenotype. Our data are consistent with the liver being a major site

352 for sulfide disposal rather than production[32]. Moreover, our data suggest that the liver of
353 *Tst*$^{-/-}$ mice has over-compensated in its response to maximise hepatic sulfide removal, thus
354 engendering detrimental metabolic consequences indirectly. This response is achieved
355 through a combination of distinct compartmentalised cellular responses including increased
356 respiratory sulfide disposal and export of cysteine and GSH and is further evidenced by the
357 reduction of global hepatic protein persulfidation and depletion of sulfide-responsive[51] NRF2
358 target proteins. Additionally, up-regulation of translation and recruitment of MPST to the
359 mitochondria of *Tst*$^{-/-}$ mice is observed. This response, in face of reduced transcription of
360 *Mpst* due to *Mpst* promoter disruption by the *Tst* null allele, suggests a powerful post-
361 transcriptional cellular sulfide sensing mechanism. Moreover, if MPST is compensating for
362 TST–mediated sulfide disposal in this context, this suggests a subversion of normal MPST
363 function away from sulfide production[52,53 54,55]. Intriguingly, TST expression levels were
364 elevated in the liver of *Mpst*$^{-/-}$ mice, providing further support for an exquisite reciprocal
365 compensatory mechanism between these two enzymes[56].
366 The unexpected finding of normal hepatic sulfide levels in the *Tst*$^{-/-}$ mice led us to discover
367 that the metabolic phenotype we observed was driven by the very mechanisms invoked to
368 maintain sulfide within a normal range rather than sulfide excess *per se*. Several observations
369 were consistent with this. For example, the major amino acid pathways increased in the liver
370 proteome of *Tst*$^{-/-}$ mice were transaminases involved in metabolism of GSH that support
371 increased export of sulfur equivalents as GSH (and cysteine). These same transaminases
372 support gluconeogenesis by redirecting Krebs cycle intermediates[57–59]. Re–programming of
373 amino acid metabolism for sulfide disposal, with knock–on effects to drive hepatic glucose
374 production are suggested, rather than any change to amino acid–linked mitochondrial
375 respiration in hepatocytes. This is supported by the shift in pyruvate metabolism towards

376 aspartate. In addition, glutathione-S-transferases (GST) that inhibit gluconeogenesis[60] were
377 lower in the liver of *Tst*$^{-/-}$ mice. Further, NRF2 activation, which represses gluconeogenesis[61]
378 appears lower in liver of *Tst*$^{-/-}$ mice. The involvement of NRF2 in the *Tst*$^{-/-}$ liver phenotype
379 is further supported by the phenotype of *Nrf2*$^{-/-}$ mice that also exhibited steatohepatitis, in
380 the absence of insulin resistance[62]. However, we note that NRF2 signalling can be complex
381 and dependent upon dietary context; *Nrf2*$^{-/-}$ mice showed improved glucose tolerance after
382 a high–fat diet[63] suggesting any contribution of a NRF2 signalling deficit in the liver of the *Tst*$^{-}$
383 $^{/-}$ mice changes upon high fat feeding. Beyond altered pyruvate flux, we also showed that the
384 hepatocytes of *Tst*$^{-/-}$ mice exhibited defective lipid metabolism. Specifically, medium–chain
385 fatty acid (MCFA) oxidation was impaired, associated with selective reduction of protein levels
386 and persulfidation levels of lipid catabolic enzymes. This represents a novel mechanism
387 linking altered sulfide metabolism to lipid oxidation, hepatic lipid accumulation and
388 dyslipidaemia. Consistent with impaired MCFA oxidation defects as a driver, at least in part,
389 of the phenotype of *Tst*$^{-/-}$ mice, steatosis is observed in medium–chain acyl-CoA
390 dehydrogenase (*Mcad*)$^{-/-}$ mice[64] and dyslipidemia is found in MCADD deficient humans[65].
391 The data we present adds to a growing understanding of the link between sulfide regulating
392 genes and nutrient metabolism that has hitherto focussed on the enzymes of sulfide
393 production. Specifically, we provide support for the importance of the sulfide oxidising
394 pathway as a regulator of cellular sulfide exposure. Unexpectedly, the data reveal novel
395 cellular mechanisms that are engaged to homeostatically regulate sulfide disposal and that
396 can impact upon cell energetics and nutrient metabolism.
397 Our findings may have implications for potentially unexpected side effects of sulfide donor
398 therapeutics. In normal mice, *in vivo* sulfide administration for 4 weeks post–HFD partially
399 reversed hepatic lipid accumulation invoked by chronic (16 weeks) HFD[22]. No evidence was

400 provided for whether sulfide disposal mechanisms were altered[22]. This efficacious sub-
401 chronic sulfide administration regimen contrasts with our genetic model of chronic sulfide
402 elevation as a driver of dysregulated metabolism and NAFLD. Clearly, the normal mice in the
403 Na_2S administration studies had a fully functional SOP, suggesting the presence of TST is
404 required to achieve the beneficial metabolic effects of Na_2S administration. This is also
405 consistent with the apparently low sulfide signalling status (evidenced by lower
406 persulfidation, NRF2 target protein abundance) in the liver of the *Tst*$^{-/-}$ mice. The benefits
407 of elevated sulfide cannot be realised, perhaps because the major mediator of those effects
408 is missing and the alternate mechanisms invoked do not fully compensate (e.g. MPST), or
409 actively drive aberrant nutrient metabolism. Comparable studies of glucose and lipid
410 metabolism after manipulation of other sulfide regulating genes are limited. However in a
411 contrasting model of reduced sulfide production (*Cth*$^{-/-}$ mice), plasma triglycerides were
412 lowered[23], consistent and opposite to what we observed with the *Tst*$^{-/-}$ mice. The hepatic
413 sulfide disposal status of the *Cth*$^{-/-}$ mouse model is unknown, but our findings predict a
414 suppression of the SOP to spare the limited endogenous sulfide produced. Intriguingly they
415 also predict a knock-on effect on nutrient homeostasis due to reduced metabolic demand of
416 the TST/SOP axis. A more direct model informing on the effects of impairment of the sulfide
417 disposal pathway is deficiency of the key mitochondrial SOP enzyme ETHE1. *Ethe1*$^{-/-}$ mice
418 suffer fatal sulfide toxicity[30] and therefore comparable metabolic studies are lacking.
419 However, one notable observation is that *Ethe1*$^{-/-}$ mice have an apparently 10-fold higher
420 liver sulfide exposure than control mice[30], in contrast to the normalised hepatic sulfide levels
421 of *Tst*$^{-/-}$ mice. Circulating sulfide levels were not reported for comparison, but the
422 presumably relatively lower systemic sulfide levels of *Tst*$^{-/-}$ mice appear to have permitted
423 an effective homeostatic sulfide disposal response in the liver to avoid toxicity, albeit with a

424 metabolic cost. Consequently, the liver of *Tst*$^{-/-}$ mice has a distinct functional and proteomic
425 profile to that of the *Ethe1*$^{-/-}$ mice. For example, in the liver of *Tst*$^{-/-}$ and *Ethe1*$^{-/-}$ mice[66],
426 proteins of the glutathione–S–transferase Mu type (GSTM) and peroxiredoxin (PRDX) families
427 were altered, but sometimes in the opposite direction or with alteration of distinct protein
428 sub-classes. A notable difference is also observed in amino acid metabolism. The liver of
429 *Ethe1*$^{-/-}$ mice exhibited increased expression of enzymes of branched chain amino acid
430 metabolism[66], distinct from the predominantly glutathione–related amino acid pathways that
431 are increased in liver of *Tst*$^{-/-}$ mice. Beyond sulfide, TST may also have distinct cellular roles
432 that affect metabolism such as mitoribosomal synthesis, ROS attenuation and modulation of
433 mitochondrial iron-sulfur clusters[67–71].
434 Given the pro-diabetogenic liver phenotype in *Tst*$^{-/-}$ mice, its was surprising that insulin
435 signalling in the liver appeared normal, and peripheral insulin sensitivity was, if anything,
436 increased. There are precedents for increased hepatic glucose production independent of
437 insulin resistance, as found in the *Nrf2*$^{-/-}$ mice[62] and as driven by the transcription factor
438 ChREBP[72,73]. There is also evidence to support insulin–sensitising effects of sulfide
439 administration *in vivo* in mice and rats[74–76], consistent with a sulfide–mediated insulin–
440 sensitisation of non-hepatic tissues in *Tst*$^{-/-}$ mice. Higher circulating GSH in *Tst*$^{-/-}$ mice may
441 also promote peripheral insulin–sensitisation[77,78]. Clearly, the net balance of glucose
442 production from the liver and its peripheral disposal remains abnormal in *Tst*$^{-/-}$ mice.
443 Indeed, the baseline metabolic phenotype of *Tst*$^{-/-}$ mice resembles in many ways that of a
444 normal mouse fed a HFD. Thus, we expected to gain insight into conserved pro-diabetogenic
445 mechanisms from the overlap between the liver proteome of *Tst*$^{-/-}$ mice and that of HFD-
446 fed C57BL/6J mice. However, upon closer inspection this was not entirely the case, with some
447 lipid metabolism and peroxisomal proteins changing in the opposite direction to those

448 observed in HFD–fed C57BL/6J mice. Unlike a HFD state, which is associated with dominant
449 hepatic insulin resistance, the increased hepatic glucose production in ND-fed *Tst*$^{-/-}$ mice
450 occurs despite of normal hepatic insulin sensitivty. The significant changes in persulfidation
451 of transaminase and gluconeogenesis proteins in the liver of *Tst*$^{-/-}$ mice suggest a
452 coordinated cross–talk across metabolic pathways underlies this atypical metabolic
453 phenotype.
454 Sulfide donor therapeutics were proposed as a clinical strategy for improving cardiovascular
455 health[27,79,80]. Elevated endogenous sulfide was also implicated in the beneficial metabolic
456 effects of caloric restriction[11,81–85]. Our results suggest that chronic sulfide elevation may have
457 unintended detrimental consequences, driving liver glucose production and fat accumulation
458 to undesirable levels. This caveat may be fortunately limited to cases where SOP proteins are
459 compromised through rare genetic effects – such as TST variants[86,87]. More broadly, a number
460 of drugs or supplements are known to increase cyanide, which may dominantly inhibit TST
461 activity and result in secondary sulfide overexposure. These include nitroprusside[88] and
462 amygdalin[89,90]. Indeed the TST metabolite thiosulfate is commonly co-administered with
463 nitroprusside to prevent cyanide toxicity[91]. Furthermore, dietary and environmental exposure
464 to cyanogenic compounds[92], e.g. smoking[93] or cyanogenic diets[94] may interfere with normal
465 TST function and could lead to increased sensitivity to sulfide therapeutics. In contrast, we
466 have shown that administration of the TST substrate thiosulfate can ameliorate diabetes[35]
467 further underlining the potential utility of targeting the SOP in metabolic disease. As with all
468 therapeutic strategies, a careful cost-benefit analysis is required. A comparable case of
469 relevance are the statins, one of the most potent and widely used drugs to prevent
470 atherosclerosis, which also carry a higher risk for diabetes[95]. The full impact of TST
471 manipulation on opposing metabolic pathways requires further study. Our current study

472 sheds light on the underlying hepatic mechanisms invoked for sulfide disposal that are
473 relevant to current sulfide–donor strategies and may inform on routes to reduce their
474 potential metabolic side-effects.
475

476 Methods

477 The methods for all data and work presented in this manuscript is provided as supplementary
478 information.

479 Author Contributions

480 N.M.M. and R.N.C conceived experiments. R.N.C., M.T.G.G, M. B.-L., A. M.-C., M.L., V.V., B.E.,
481 T. LeB., M.B., S.H., S.D., N.H., C. Mc F., A.T., N. F., T.G., performed experiments. R.N.C., M. B.-
482 L., P.F., V.V., T. LeB., N.H., T.S., F.B., T.G., R.C.H., B.S., G.G., A.J.F., C.S., R.B. and N.M.M.
483 analysed and interpreted data and commented on the manuscript. K.H.A., S.S. generated
484 reagents. C.McM. and R.C.H. generated reagents. R.N.C. and N.M.M. wrote the manuscript.

485 Acknowledgements

486 This work was funded by a Wellcome Trust New Investigator Award to NMM (100981/Z/13/Z)
487 and Diabetes UK grant (17/0005697). RCH was funded by a Medical Research Council
488 Discovery Award (MC-PC-15076). We would like to thank Professor Ken Olsen and Eric DeLeon
489 (Notre Dame) for advice establishing sulfide measurement by probe.

490

491

492 # References

493 1. OMS. GLOBAL REPORT ON DIABETES WHO Library Cataloguing-in-Publication Data.
494 *ISBN*. 2014;978:92-94. http://www.who.int/about/licensing/.
495 2. Lewis GF, Carpentier A, Adeli K, Giacca A. Disordered fat storage and mobilization in
496 the pathogenesis of insulin resistance and type 2 diabetes. *Endocr Rev*.
497 2002;23(2):201-229. doi:10.1210/edrv.23.2.0461
498 3. Consoli A, Nurjhan N, Capani F, Gerich J. Predominant role of gluconeogenesis in
499 increased hepatic glucose production in NIDDM. *Diabetes*. 1989;38(5):550-557.
500 doi:10.2337/diab.38.5.550
501 4. Caron S, Verrijken A, Mertens I, et al. Transcriptional activation of apolipoprotein CIII
502 expression by glucose may contribute to diabetic dyslipidemia. *Arterioscler Thromb*
503 *Vasc Biol*. 2011;31(3):513-519. doi:10.1161/ATVBAHA.110.220723
504 5. Abe K, Kimura H. The possible role of hydrogen sulfide as an endogenous
505 neuromodulator. *J Neurosci*. 1996;16(3):1066-1071.
506 http://www.ncbi.nlm.nih.gov/pubmed/8558235.
507 6. Wang R. Physiological Implications of Hydrogen Sulfide: A Whiff Exploration That
508 Blossomed. *Physiol Rev*. 2012;92(2):791-896. doi:10.1152/physrev.00017.2011
509 7. Mishanina T V., Libiad M, Banerjee R. Biogenesis of reactive sulfur species for
510 signaling by hydrogen sulfide oxidation pathways. *Nat Chem Biol*. 2015;11(7):457-
511 464. doi:10.1038/nchembio.1834
512 8. Filipovic MR, Zivanovic J, Alvarez B, Banerjee R. Chemical Biology of H2S Signaling
513 through Persulfidation. *Chem Rev*. 2017. doi:10.1021/acs.chemrev.7b00205
514 9. Desai KM, Chang T, Untereiner A, Wu L. Hydrogen sulfide and the metabolic

515 syndrome. *Expert Rev Clin Pharmacol*. 2011;4(1):63-73. doi:10.1586/ecp.10.133

516 10. Szabo C. Roles of Hydrogen Sulfide in the Pathogenesis of Diabetes Mellitus and Its
517 Complications. *Antioxid Redox Signal*. 2011;17(1):68-80. doi:10.1089/ars.2011.4451

518 11. Hine C, Harputlugil E, Zhang Y, et al. Endogenous hydrogen sulfide production is
519 essential for dietary restriction benefits. *Cell*. 2015. doi:10.1016/j.cell.2014.11.048

520 12. Carter RN, Morton NM. Cysteine and hydrogen sulphide in the regulation of
521 metabolism: Insights from genetics and pharmacology. *J Pathol*. 2016;238(2):321-332.
522 doi:10.1002/path.4659

523 13. Chen X, Jhee KH, Kruger WD. Production of the neuromodulator H2S by
524 cystathionine ??-synthase via the condensation of cysteine and homocysteine. *J Biol*
525 *Chem*. 2004. doi:10.1074/jbc.C400481200

526 14. Singh S, Padovani D, Leslie RA, Chiku T, Banerjee R. Relative contributions of
527 cystathionine ??-synthase and ??-cystathionase to H2S biogenesis via alternative
528 trans-sulfuration reactions. *J Biol Chem*. 2009. doi:10.1074/jbc.M109.010868

529 15. Shibuya N, Tanaka M, Yoshida M, et al. 3-Mercaptopyruvate Sulfurtransferase
530 Produces Hydrogen Sulfide and Bound Sulfane Sulfur in the Brain. *Antioxid Redox*
531 *Signal*. 2009. doi:10.1089/ars.2008.2253

532 16. Mikami Y, Shibuya N, Kimura Y, Nagahara N, Ogasawara Y, Kimura H. Thioredoxin and
533 dihydrolipoic acid are required for 3-mercaptopyruvate sulfurtransferase to produce
534 hydrogen sulfide. *Biochem J*. 2011. doi:10.1042/BJ20110841

535 17. Yadav PK, Yamada K, Chiku T, Koutmos M, Banerjee R. Structure and kinetic analysis
536 of H2S production by human mercaptopyruvate sulfurtransferase. *J Biol Chem*. 2013.
537 doi:10.1074/jbc.M113.466177

538 18. Wedmann R, Onderka C, Wei S, et al. Improved tag-switch method reveals that

539 thioredoxin acts as depersulfidase and controls the intracellular levels of protein
540 persulfidation. *Chem Sci*. 2016;7(5):3414-3426. doi:10.1039/c5sc04818d
541 19. Mani S, Cao W, Wu L, Wang R. Hydrogen sulfide and the liver. *Nitric Oxide - Biol*
542 *Chem*. 2014. doi:10.1016/j.niox.2014.02.006
543 20. Pichette J, Gagnon J. Implications of Hydrogen Sulfide in Glucose Regulation: How
544 H2S Can Alter Glucose Homeostasis through Metabolic Hormones. *Oxid Med Cell*
545 *Longev*. 2016;2016. doi:10.1155/2016/3285074
546 21. Zhang L, Yang G, Untereiner A, Ju Y, Wu L, Wang R. Hydrogen sulfide impairs glucose
547 utilization and increases gluconeogenesis in hepatocytes. *Endocrinology*. 2013.
548 doi:10.1210/en.2012-1658
549 22. Wu D, Zheng N, Qi K, et al. Exogenous hydrogen sulfide mitigates the fatty liver in
550 obese mice through improving lipid metabolism and antioxidant potential. *Med Gas*
551 *Res*. 2015;5(1). doi:10.1186/s13618-014-0022-y
552 23. Mani S, Li H, Untereiner A, et al. Decreased endogenous production of hydrogen
553 sulfide accelerates atherosclerosis. *Circulation*. 2013;127(25):2523-2534.
554 doi:10.1161/CIRCULATIONAHA.113.002208
555 24. Distrutti E, Mencarelli A, Santucci L, et al. The methionine connection: Homocysteine
556 and hydrogen sulfide exert opposite effects on hepatic microcirculation in rats.
557 *Hepatology*. 2008;47(2):659-667. doi:10.1002/hep.22037
558 25. Fiorucci S, Antonelli E, Mencarelli A, et al. The third gas: H2S regulates perfusion
559 pressure in both the isolated and perfused normal rat liver and in cirrhosis.
560 *Hepatology*. 2005;42(3):539-548. doi:10.1002/hep.20817
561 26. Sestito S, Nesi G, Pi R, Macchia M, Rapposelli S. Hydrogen Sulfide: A Worthwhile Tool
562 in the Design of New Multitarget Drugs. *Front Chem*. 2017;5.

563 doi:10.3389/fchem.2017.00072

564 27. Whiteman M, Le Trionnaire S, Chopra M, Fox B, Whatmore J. Emerging role of
565 hydrogen sulfide in health and disease: critical appraisal of biomarkers and
566 pharmacological tools. *Clin Sci*. 2011;121(11):459-488. doi:10.1042/cs20110267

567 28. Libiad M, Motl N, Akey DL, et al. Thiosulfate Sulfurtransferase like Domain Containing
568 1 Protein Interacts with Thioredoxin. *J Biol Chem*. January 2018:jbc.RA117.000826.
569 doi:10.1074/jbc.RA117.000826

570 29. Reiffenstein R. Toxicology Of Hydrogen Sulfide. *Annu Rev Pharmacol Toxicol*.
571 1992;32(1):109-134. doi:10.1146/annurev.pharmtox.32.1.109

572 30. Tiranti V, Viscomi C, Hildebrandt T, et al. Loss of ETHE1, a mitochondrial dioxygenase,
573 causes fatal sulfide toxicity in ethylmalonic encephalopathy. *Nat Med*.
574 2009;15(2):200-205. doi:10.1038/nm.1907

575 31. Hildebrandt TM, Grieshaber MK. Three enzymatic activities catalyze the oxidation of
576 sulfide to thiosulfate in mammalian and invertebrate mitochondria. *FEBS J*.
577 2008;275(13):3352-3361. doi:10.1111/j.1742-4658.2008.06482.x

578 32. Norris EJ, Culberson CR, Narasimhan S, Clemens MG. The liver as a central regulator
579 of hydrogen sulfide. *Shock*. 2011. doi:10.1097/SHK.0b013e3182252ee7

580 33. Jackson MR, Melideo SL, Jorns MS. Human sulfide:Quinone oxidoreductase catalyzes
581 the first step in hydrogen sulfide metabolism and produces a sulfane sulfur
582 metabolite. *Biochemistry*. 2012. doi:10.1021/bi300778t

583 34. Libiad M, Yadav PK, Vitvitsky V, Martinov M, Banerjee R. Organization of the human
584 mitochondrial hydrogen sulfide oxidation pathway. *J Biol Chem*. 2014.
585 doi:10.1074/jbc.M114.602664

586 35. Morton NM, Beltram J, Carter RN, et al. Genetic identification of thiosulfate

587 sulfurtransferase as an adipocyte-expressed antidiabetic target in mice selected for
588 leanness. *Nat Med*. 2016;22(7). doi:10.1038/nm.4115
589 36. Gero, Domokos Torregrossa R, Perry A, Waters A, et al. The novel mitochondria-
590 targeted hydrogen sulfide (H2S) donors AP123 and AP39 protect against
591 hyperglycemic injury in microvascular endothelial cells in vitro. *Pharmacol Res*.
592 2016;113:186-198.
593 https://reader.elsevier.com/reader/sd/pii/S1043661816306314?token=3623BE15023
594 42420421E3956873F1E65FD3FCBDE1D675D7396DB26A…1/13.
595 37. Karwi QG, Bice JS, Baxter GF. Pre- and postconditioning the heart with hydrogen
596 sulfide (H2S) against ischemia/reperfusion injury in vivo: a systematic review and
597 meta-analysis. *Basic Res Cardiol*. 2018;113(1). doi:10.1007/s00395-017-0664-8
598 38. Mason TM. The role of factors that regulate the synthesis and secretion of very-low-
599 density lipoprotein by hepatocytes. *Crit Rev Clin Lab Sci*. 1998;35(6):461-487.
600 doi:10.1080/10408369891234246
601 39. Vitvitsky V, Yadav PK, Kurthen A, Banerjee R. Sulfide oxidation by a noncanonical
602 pathway in red blood cells generates thiosulfate and polysulfides. *J Biol Chem*.
603 2015;290(13):8310-8320. doi:10.1074/jbc.M115.639831
604 40. Vitvitsky V, Yadav PK, An S, Seravalli J, Cho US, Banerjee R. Structural and mechanistic
605 insights into hemoglobincatalyzed hydrogen sulfide oxidation and the fate of
606 polysulfide products. *J Biol Chem*. 2017. doi:10.1074/jbc.M117.774943
607 41. Banerjee R, Chiku T, Kabil O, Libiad M, Motl N, Yadav PK. *Assay Methods for H2S*
608 *Biogenesis and Catabolism Enzymes*. Vol 554. Academic Press Inc.; 2015:189-200.
609 doi:10.1016/bs.mie.2014.11.016
610 42. Singha S, Kim D, Moon H, et al. Toward a selective, sensitive, fast-responsive, and

611 biocompatible two-photon probe for hydrogen sulfide in live cells. *Anal Chem*.
612 2015;87(2):1188-1195. doi:10.1021/ac503806w
613 43. Arndt S, Baeza-Garza CD, Logan A, et al. Assessment of H 2 S in vivo using the newly
614 developed mitochondria-targeted mass spectrometry probe MitoA. *J Biol Chem*.
615 2017;292(19):7761-7773. doi:10.1074/jbc.M117.784678
616 44. Krishnan N, Fu C, Pappin DJ, Tonks NK. H2S-Induced Sulfhydration of the Phosphatase
617 PTP1B and Its Role in the Endoplasmic Reticulum Stress Response. *Sci Signal*. 2011.
618 doi:10.1126/scisignal.2002329
619 45. Kabil O, Motl N, Banerjee R. H2S and its role in redox signaling. *Biochim Biophys Acta -*
620 *Proteins Proteomics*. 2014;1844(8):1355-1366. doi:10.1016/j.bbapap.2014.01.002
621 46. Koike S, Nishimoto S, Ogasawara Y. Cysteine persulfides and polysulfides produced by
622 exchange reactions with H2S protect SH-SY5Y cells from methylglyoxal-induced
623 toxicity through Nrf2 activation. *Redox Biol*. 2017;12:530-539.
624 doi:10.1016/j.redox.2017.03.020
625 47. Nagahara N. Catalytic Site Cysteines of Thiol Enzyme: Sulfurtransferases. *J Amino*
626 *Acids*. 2011. doi:10.4061/2011/709404
627 48. Batista TM, Garcia-Martin R, Cai W, et al. Multi-dimensional Transcriptional
628 Remodeling by Physiological Insulin In Vivo. *Cell Rep*. 2019;26(12):3429-3443.e3.
629 doi:10.1016/j.celrep.2019.02.081
630 49. Sutherland C, O'Brien R, Granner D. *Insulin Action Gene Regulation. In: Madame*
631 *Curies Bioscience Database [Internet].* Austin(TX); 2013.
632 https://www.ncbi.nlm.gov/books/NBK6471.
633 50. Xie L, Gu Y, Wen M, et al. Hydrogen sulfide induces Keap1 S-sulfhydration and
634 suppresses diabetes-accelerated atherosclerosis via Nrf2 activation. *Diabetes*.

635 2016;65(10):3171-3184. doi:10.2337/db16-0020

636 51. Yang G, Zhao K, Ju Y, et al. Hydrogen sulfide protects against cellular senescence via s-
637 sulfhydration of keap1 and activation of Nrf2. *Antioxidants Redox Signal*.
638 2013;18(15):1906-1919. doi:10.1089/ars.2012.4645

639 52. Módis K, Coletta C, Erdélyi K, Papapetropoulos A, Szabo C. Intramitochondrial
640 hydrogen sulfide production by 3-mercaptopyruvate sulfurtransferase maintains
641 mitochondrial electron flow and supports cellular bioenergetics. *FASEB J*. 2013.
642 doi:10.1096/fj.12-216507

643 53. Szabo C, Ransy C, Módis K, et al. Regulation of mitochondrial bioenergetic function by
644 hydrogen sulfide. Part I. Biochemical and physiological mechanisms. *Br J Pharmacol*.
645 2014. doi:10.1111/bph.12369

646 54. Nagahara N. Multiple role of 3-mercaptopyruvate sulfurtransferase: antioxidative
647 function, H2S and polysulfide production and possible SOx production. *Br J*
648 *Pharmacol*. 2018;175(4):577-589. doi:10.1111/bph.14100

649 55. Kimura Y, Koike S, Shibuya N, Lefer D, Ogasawara Y, Kimura H. 3-Mercaptopyruvate
650 sulfurtransferase produces potential redox regulators cysteine- and glutathione-
651 persulfide (Cys-SSH and GSSH) together with signaling molecules H 2 S 2 , H 2 S 3 and
652 H 2 S. *Sci Rep*. 2017;7(1):1-14. doi:10.1038/s41598-017-11004-7

653 56. Nagahara N, Tanaka M, Tanaka Y, Ito T. Novel Characterization of Antioxidant
654 Enzyme, 3-Mercaptopyruvate Sulfurtransferase-Knockout Mice: Overexpression of
655 the Evolutionarily-Related Enzyme Rhodanese. *Antioxidants*. 2019;8(5):116.
656 doi:10.3390/antiox8050116

657 57. Rui L. Energy metabolism in the liver. *Compr Physiol*. 2014;4(1):177-197.
658 doi:10.1002/cphy.c130024

659 58. Qian K, Zhong S, Xie K, Yu D, Yang R, Gong DW. Hepatic ALT isoenzymes are elevated
660 in gluconeogenic conditions including diabetes and suppressed by insulin at the
661 protein level. *Diabetes Metab Res Rev*. 2015;31(6):562-571. doi:10.1002/dmrr.2655
662 59. Sookoian S, Castaño GO, Scian R, et al. Serum aminotransferases in nonalcoholic fatty
663 liver disease are a signature of liver metabolic perturbations at the amino acid and
664 Krebs cycle level. *Am J Clin Nutr*. 2016;103(2):422-434. doi:10.3945/ajcn.115.118695
665 60. Ghosh Dastidar S, Jagatheesan G, Haberzettl P, et al. Glutathione S -transferase P
666 deficiency induces glucose intolerance via JNK-dependent enhancement of hepatic
667 gluconeogenesis . *Am J Physiol Metab*. 2018;315(5):E1005-E1018.
668 doi:10.1152/ajpendo.00345.2017
669 61. Slocum SL, Skoko JJ, Wakabayashi N, et al. Keap1/Nrf2 pathway activation leads to a
670 repressed hepatic gluconeogenic and lipogenic program in mice on a high-fat diet.
671 *Arch Biochem Biophys*. 2016;591:57-65. doi:10.1016/j.abb.2015.11.040
672 62. Meakin PJ, Chowdhry S, Sharma RS, et al. Susceptibility of Nrf2-Null Mice to
673 Steatohepatitis and Cirrhosis upon Consumption of a High-Fat Diet Is Associated with
674 Oxidative Stress, Perturbation of the Unfolded Protein Response, and Disturbance in
675 the Expression of Metabolic Enzymes but Not with Insulin Resistance. *Mol Cell Biol*.
676 2014;34(17):3305-3320. doi:10.1128/mcb.00677-14
677 63. Zhang YKJ, Wu KC, Liu J, Klaassen CD. Nrf2 deficiency improves glucose tolerance in
678 mice fed a high-fat diet. *Toxicol Appl Pharmacol*. 2012;264(3):305-314.
679 doi:10.1016/j.taap.2012.09.014
680 64. Tolwani RJ, Hamm DA, Tian L, et al. Medium-chain acyl-CoA dehydrogenase deficiency
681 in gene-targeted mice. *PLoS Genet*. 2005;1(2):0205-0212.
682 doi:10.1371/journal.pgen.0010023

683 65. Onkenhout W, Venizelos V, Van Der Poet PFH, Van Den Heuvel MPM, Poorthuis
684 BJHM. *Identification and Quantification of Intermediates of Unsaturated Fatty Acid*
685 *Metabolism in Plasma of Patients with Fatty Acid Oxidation Disorders*. Vol 10.; 1995.
686 66. Hildebrandt TM, Di Meo I, Zeviani M, Viscomi C, Braun H. Proteome adaptations in
687 Ethe1-deficient mice indicate a role in lipid catabolism and cytoskeleton organization
688 via post-translational protein modifications. *Biosci Rep*. 2013;33(4):575-584.
689 doi:10.1042/bsr20130051
690 67. Bonomi F, Pagani S, Cerletti P, Cannella C. *Rhodanese-Mediated Sulfur Transfer to*
691 *Succinate Dehydrogenase*. Vol 72.; 1977.
692 68. Pagani S, Galante YM. *INTERACTION OF RHODANESE WITH MITOCHONDRIAL NADH*
693 *DEHYDROGENASE*. Vol 742.; 1983.
694 69. Nandi DL, Westley J. Reduced thioredoxin as a sulfur-acceptor substrate for
695 rhodanese. *Int J Biochem Cell Biol*. 1998. doi:10.1016/S1357-2725(98)00050-8
696 70. Nandi DL, Horowitz PM, Westley J. Rhodanese as a thioredoxin oxidase. *Int J Biochem*
697 *Cell Biol*. 2000;32(4):465-473. doi:10.1016/S1357-2725(99)00035-7
698 71. Smirnov A, Comte C, Mager-Heckel AM, et al. Mitochondrial enzyme rhodanese is
699 essential for 5 S ribosomal RNA import into human mitochondria. *J Biol Chem*.
700 2010;285(40):30792-30803. doi:10.1074/jbc.M110.151183
701 72. Uyeda K, Repa JJ. Carbohydrate response element binding protein, ChREBP, a
702 transcription factor coupling hepatic glucose utilization and lipid synthesis. *Cell*
703 *Metab*. 2006;4(2):107-110. doi:10.1016/j.cmet.2006.06.008
704 73. Kim MS, Krawczyk SA, Doridot L, et al. ChREBP regulates fructose-induced glucose
705 production independently of insulin signaling. *J Clin Invest*. 2016;126(11):4372-4386.
706 doi:10.1172/JCI81993

707 74. Xue R, Hao D-D, Sun J-P, et al. Hydrogen Sulfide Treatment Promotes Glucose Uptake
708 by Increasing Insulin Receptor Sensitivity and Ameliorates Kidney Lesions in Type 2
709 Diabetes. *Antioxid Redox Signal*. 2013;19(1):5-23. doi:10.1089/ars.2012.5024
710 75. Feng X, Chen Y, Zhao J, Tang C, Jiang Z, Geng B. Hydrogen sulfide from adipose tissue
711 is a novel insulin resistance regulator. *Biochem Biophys Res Commun*. 2009.
712 doi:10.1016/j.bbrc.2009.01.059
713 76. Geng B, Cai B, Liao F, et al. Increase or Decrease Hydrogen Sulfide Exert Opposite
714 Lipolysis, but Reduce Global Insulin Resistance in High Fatty Diet Induced Obese Mice.
715 *PLoS One*. 2013;8(9). doi:10.1371/journal.pone.0073892
716 77. Lutchmansingh FK, Hsu JW, Bennett FI, et al. Glutathione metabolism in type 2
717 diabetes and its relationship with microvascular complications and glycemia. *PLoS*
718 *One*. 2018;13(6). doi:10.1371/journal.pone.0198626
719 78. Jain SK, Micinski D, Huning L, Kahlon G, Bass PF, Levine SN. Vitamin D and L-cysteine
720 levels correlate positively with GSH and negatively with insulin resistance levels in the
721 blood of type 2 diabetic patients. *Eur J Clin Nutr*. 2014;68(10):1148-1153.
722 doi:10.1038/ejcn.2014.114
723 79. Zhang L, Wang Y, Li Y, et al. Hydrogen sulfide (H2S)-releasing compounds: Therapeutic
724 potential in cardiovascular diseases. *Front Pharmacol*. 2018;9(SEP).
725 doi:10.3389/fphar.2018.01066
726 80. Szabó G, Veres G, Radovits T, et al. Cardioprotective effects of hydrogen sulfide. In:
727 *Nitric Oxide - Biology and Chemistry*. Vol 25. ; 2011:201-210.
728 doi:10.1016/j.niox.2010.11.001
729 81. Miller RA, Buehner G, Chang Y, Harper JM, Sigler R, Smith-Wheelock M. Methionine-
730 deficient diet extends mouse lifespan, slows immune and lens aging, alters glucose,

731 T4, IGF-I and insulin levels, and increases hepatocyte MIF levels and stress resistance.
732 *Aging Cell*. 2005. doi:10.1111/j.1474-9726.2005.00152.x
733 82. Lee BC, Kaya A, Gladyshev VN. Methionine restriction and life-span control. *Ann N Y*
734 *Acad Sci*. 2016. doi:10.1111/nyas.12973
735 83. Shimokawa I, Komatsu T, Hayashi N, et al. The life-extending effect of dietary
736 restriction requires Foxo3 in mice. *Aging Cell*. 2015. doi:10.1111/acel.12340
737 84. Hine C, Kim HJ, Zhu Y, et al. Hypothalamic-Pituitary Axis Regulates Hydrogen Sulfide
738 Production. *Cell Metab*. 2017. doi:10.1016/j.cmet.2017.05.003
739 85. Hine C, Zhu Y, Hollenberg AN, Mitchell JR. Dietary and Endocrine Regulation of
740 Endogenous Hydrogen Sulfide Production: Implications for Longevity. *Antioxid Redox*
741 *Signal*. 2018;28(16):1483-1502. doi:10.1089/ars.2017.7434
742 86. Libiad M, Sriraman A, Banerjee R. Polymorphic variants of human rhodanese exhibit
743 differences in thermal stability and sulfur transfer kinetics. *J Biol Chem*. 2015.
744 doi:10.1074/jbc.M115.675694
745 87. Billaut-Laden I, Allorge D, Crunelle-Thibaut A, et al. Evidence for a functional genetic
746 polymorphism of the human thiosulfate sulfurtransferase (Rhodanese), a cyanide and
747 H2S detoxification enzyme. *Toxicology*. 2006;225(1):1-11.
748 doi:10.1016/j.tox.2006.04.054
749 88. Morris AA, Page RL, Baumgartner LJ, et al. Thiocyanate Accumulation in Critically Ill
750 Patients Receiving Nitroprusside Infusions. *J Intensive Care Med*. 2017;32(9):547-553.
751 doi:10.1177/0885066616657004
752 89. Bromley J, Hughes BGM, Leong DCS, Buckley NA. Life-threatening interaction
753 between complementary medicines: Cyanide toxicity following ingestion of
754 amygdalin and vitamin C. *Ann Pharmacother*. 2005;39(9):1566-1569.

755 doi:10.1345/aph.1E634

756 90. O'brien B, Quigg C, Leong T. *Severe Cyanide Toxicity from "Vitamin Supplements."* Vol
757 12. Lippincott Williams & Wilkins; 2005.
758 http://www.cancer.gov/cancerinfo/pdq/cam.laetrile.

759 91. Curry SC, Carlton MW, Raschke RA. Prevention of fetal and maternal cyanide toxicity
760 from nitroprusside with coinfusion of sodium thiosulfate in gravid ewes. *Anesth*
761 *Analg*. 1997;84(5):1121-1126. doi:10.1213/00000539-199705000-00031

762 92. Petrova F. Hydrogen cyanide and cyanides : human health aspects. 2004:67.

763 93. Vinnakota C V., Peetha NS, Perrizo MG, et al. Comparison of cyanide exposure
764 markers in the biofluids of smokers and non-smokers. *Biomarkers*. 2012;17(7):625-
765 633. doi:10.3109/1354750X.2012.709880

766 94. Kashala-Abotnes E, Okitundu D, Mumba D, Boivin MJ, Tylleskär T, Tshala-Katumbay D.
767 Konzo: a distinct neurological disease associated with food (cassava) cyanogenic
768 poisoning. *Brain Res Bull*. 2019;145:87-91. doi:10.1016/j.brainresbull.2018.07.001

769 95. Swerdlow DI, Preiss D, Kuchenbaecker KB, et al. HMG-coenzyme A reductase
770 inhibition, type 2 diabetes, and bodyweight: Evidence from genetic analysis and
771 randomised trials. *Lancet*. 2015;385(9965):351-361. doi:10.1016/S0140-
772 6736(14)61183-1

773

774

775

776

777

778

Tables

Table 1. Sulfur species in blood, urine, tissue and cells	C57Bl/6J	*Tst*$^{-/-}$	*Tst*$^{-/-}$/6J ratio	Significance
A Trunk Blood (Micromolar)				
MBB-S (Sulfide)	2.28 +/- 0.43	22.18 +/- 0.85	9.73	****
MBB-SSO3 (Thiosulfate)	n.d.	6.25 +/- 3.17	n.c.	**ns**
B Trunk Plasma (Micromolar)				
MBB-S (Sulfide)	1.88 +/- 0.64	24.50 +/- 2.02	13.03	****
MBB-SSO3 (Thiosulfate)	3.99 +/- 0.99	80.29 +/- 13.6	20.12	**
MBB-GSH (reduced Glutathione)	48.0 +/- 1.15	86.25 +/- 6.27	1.80	***
C Urine (Micromoles/creatine/24hrs)				
MBB-SSO3 (Thiosulfate)	4.99 +/- 2.6	2374 +/- 319	475.75	****
D Inferior Vena Cava (Micromolar)				
MBB-S (Sulfide)	1.22 +/- 0.20	3.58 +/- 0.87	2.93	**ns (0.08)**
MBB-SSO3 (Thiosulfate)	6.58 +/- 4.51	88.3 +/- 13.0	13.42	*
E Liver (µmoles/kg wet liver)				
MBB-S (Sulfide)	13 +/- 1	17 +/- 3	1.31	**ns**
MBB-SSO3 (Thiosulfate)	4 +/- 1	15 +/- 7	3.75	**ns**
DNFB-GSH (reduced Glutathione)	6470 +/- 380	6850 +/- 30	1.04	**ns**
DNFB-Cysteine (Cysteine)	82 +/- 13	67 +/- 11	0.82	**ns**
F Sulfide P3 fluorescence (A510nm/protein)				
Hepatocyte	7.22 +/- 1.00	7.89 +/- 0.80	1.09	**ns**
G Mitochondrial sulfide (MitoA)				
Liver	0.78 +/- 0.16	1.14 +/- 0.45	1.46	**ns**
*** P < 0.05, ** P < 0.01, *** P < 0.001 **** P < 0.0001**				

Table 1. *Tst* deletion results in altered sulfur metabolites in blood and liver. (**A**) Sulfide dibimane, thiosulfate-MBB, measured by fluorescence detection following HPLC, from whole blood taken from trunk blood of ND-fed C57Bl/6J (n = 4) and *Tst*$^{-/-}$ (n = 4) mice. (**B**) Sulfide dibimane, thiosulfate-MBB, and rGSH-MBB, measured by fluorescence detection following HPLC, from EDTA-Plasma of ND-fed C57Bl/6J (n = 4) and *Tst*$^{-/-}$ (n = 4) mice. (**C**) Thiosulfate-MBB corrected for creatinine from 24 hour urine samples, taken from ND-fed C57Bl6/J (n = 4) and *Tst*$^{-/-}$ (n = 5) mice. (**D**) Sulfide dibimane, and thiosulfate-MBB, from whole blood taken from the inferior vena cava downstream of the hepatic vein of ND-fed C57Bl/6J (n = 3) and *Tst*$^{-/-}$ (n = 3) mice. (**E**) Sulfide dibimane, thiosulfate-MBB, rGSH-MBB, and cysteine-MBB from whole liver (n=4/genotype) of ND-fed C57Bl/6J (n = 4) and *Tst*$^{-/-}$ (n = 4) mice. (**F**) Fluorescence from cultured hepatocytes following incubation with P3 (sulfide reactive probe) from ND-fed C57Bl/6J (n = 4) and *Tst*$^{-/-}$ (n = 4) mice. (**G**) Ratio of Mito N/MitoA from the liver of ND-fed C57Bl/6J (n = 5) and *Tst*$^{-/-}$ (n = 5) mice. Data are represented as mean ±SEM. Significance was calculated using unpaired two-tailed student's t-test. * P < 0.05, ** P < 0.01, *** P < 0.001, **** P < 0.0001

Table 2. GO Terms persulfidation rate (*Tst*$^{-/-}$ vs C57Bl/6J liver, ND-fed)			
GO-ID	**Name**	**Direction (*Tst*$^{-/-}$ vs 6J)**	**Genes**
	GO terms Identified by log fold change		
0050660	FAD binding	Decreased	12
0008168	Methyltransferase activity	Decreased	9
0016741	Transferase activity, transferring one-carbon groups	Decreased	9
0008565	Protein transporter activity	Decreased	8
0008238	Exopeptidase activity	Decreased	7
0005777	Peroxisome	Decreased	7
0042579	Microbody	Decreased	7
0003995	Acyl-CoA dehydrogenase activity	Decreased	6
0008483	Transaminase activity	Decreased	6
0016769	Transferase activity, transferring nitrogenous groups	Decreased	6
0008757	S-adenosylmethionine-dependent methyltransferase activity	Decreased	6
0016655	Oxidoreductase activity, acting on NADH/NADPH, quinone	Decreased	5
0004177	Aminopeptidase activity	Decreased	5
0000059	Protein import into nucleus, docking	Decreased	3
0005643	Nuclear pore	Decreased	3
0031965	Nuclear membrane	Decreased	3
0044453	Nuclear membrane part	Decreased	3
0046930	Pore complex	Decreased	3
0015629	Actin cytoskeleton	Decreased	3
0016652	Oxidoreductase activity, NADH/NADPH, NAD/NADP acceptor	Decreased	3
0050662	Coenzyme binding	Increased	5
0016651	Oxidoreductase activity, NADH/NADPH,	Increased	5
0003954	NADH dehydrogenase activity	Increased	4
0008137	NADH dehydrogenase (ubiquinone) activity	Increased	4
0050136	NADH dehydrogenase (quinone) activity	Increased	4
0006739	NADP metabolism	Increased	3
0006769	Nicotinamide metabolism	Increased	3
0006733	Oxidoreduction coenzyme metabolism	Increased	3

796

797 **Table 2. Tst deletion results in differential persulfidation rate of liver proteins**. Significant GO terms
798 represented by peptides with different persulfidation rates in the ND-fed *Tst*$^{-/-}$ liver relative to
799 C57Bl/6J. '**Direction**' indicates whether the persulfidation is decreased or increased in *Tst*$^{-/-}$ relative
800 to C57Bl/6J. '**Genes**' indicates the number of genes in the *Tst*$^{-/-}$ that represent the changes driving
801 the GO term.
802

803

804

805

806

Table 3. KEGG pathways (*Tst*$^{-/-}$ vs C57Bl/6J liver, ND-fed)			
Entry	**Name**	**Genes**	**Significance**
A. Increased in ND *Tst*$^{-/-}$ liver			
00250	Alanine, aspartate and glutamate metabolism	6	***
00260	Glycine, serine and threonine metabolism	5	**
00270	Cysteine and methionine metabolism	4	*
04122	Sulfur relay system	2	*
B. Reduced in ND *Tst*$^{-/-}$ liver			
00980	Metabolism of xenobiotics by cytochrome P450	12	****
00982	Drug metabolism – cytochrome P450	12	****
05204	Chemical carcinogenesis	12	****
00480	Glutathione metabolism	8	***
00040	Pentose and glucoronate interconversions	5	**
04142	Lysosome	6	**
04390	Hippo signalling pathway	4	**
00500	Starch and sucrose metabolism	5	**
05215	Prostate cancer	3	**
04024	cAMP signalling pathway	4	*
04141	Protein processing in ER	9	*
05211	Renal cell carcinoma	3	*
00830	Retinol metabolism	6	*
00053	Ascorbate and aldarate metabolism	4	*
00860	Porphyrin and chlorophyll metabolism	4	*
04722	Neurotrophin signalling pathway	3	*
04670	Leukocyte transendothelial migration	4	*
04010	MAPK signalling pathway	4	*
04720	Long-term potentiation	2	*
04914	Progesterone-mediated oocyte maturation	2	*
04062	Chemokine signalling pathway	3	*
04110	Cell cycle	3	*
04015	Rap1 signaling pathway	4	*
00983	Drug metabolism - other enzymes	5	*
04918	Thyroid hormone synthesis	3	*
04612	Antigen processing and presentation	3	*
05203	Viral carcinogenesis	5	*
*** P < 0.05, ** P < 0.01, *** P < 0.001 **** P < 0.0001**			

807

808 **Table 3. Tst deletion results in differential hepatic protein abundance of KEGG pathways.** (**A**)
809 Significant KEGG pathway terms represented by proteins that are more abundant in the ND-fed *Tst*$^{-}$
810 $^{/-}$ liver compared with ND-fed C57Bl/6J. (**B**) Significant KEGG pathway terms represented by proteins
811 that are less abundant in the ND-fed *Tst*$^{-/-}$ liver compared with ND-fed C57Bl/6J. '**Genes**' indicates
812 the number of genes in the *Tst*$^{-/-}$ that represent the changes driving the KEGG pathway.

813

814

815

Table 4. GO Terms: Congruence of peptide abundance and persulfidation

GO-ID	Name	Persulfidation ($Tst^{-/-}$ vs 6J)	Abundance ($Tst^{-/-}$ vs 6J)
0008483	Transaminase activity	Decreased	Increased
0016769	Transferase activity, transferring nitrogenous	Decreased	Increased
0003995	Acyl-CoA dehydrogenase activity	Decreased	Decreased
0005777	Peroxisome	Decreased	Decreased
0042579	Microbody	Decreased	Decreased

816
817 **Table 4. The *Tst*$^{-/-}$ liver proteome and persulfidome converges on lipid oxidation pathways.** GO
818 terms that are significantly regulated following comparison of ND-fed *Tst*$^{-/-}$ relative to C57Bl/6J, at
819 *both* the level of cysteine persulfidation and protein abundance.
820
821
822
823
824
825
826
827
828
829
830
831
832
833
834
835
836

Figures and Legends

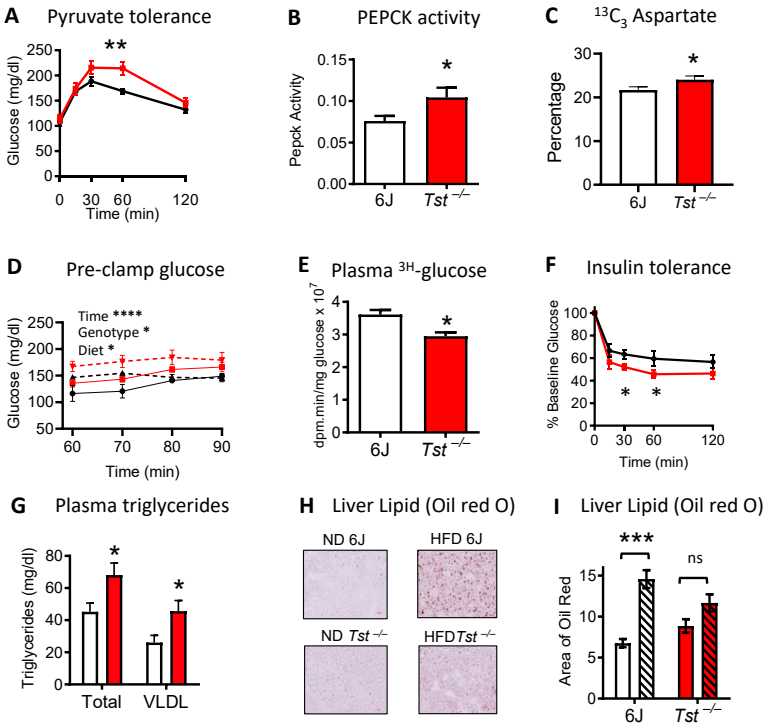

Figure 1. *Tst* deletion results in impaired glucose and lipid metabolism. (**A**) Plasma glucose over 120 minutes, following pyruvate (i.p., 1.5mg/g) administration in overnight fasted C57Bl/6J (black line, n = 9) and *Tst*$^{-/-}$ (red line, n = 8) normal diet-fed mice. (**B**) Extinction of NADH measured by absorbance at 340nm, coupled to PEPCK activity from liver homogenates taken from C57Bl/6J (white bar, n = 6) and *Tst*$^{-/-}$ (red bar, n = 6) normal diet-fed mice. (**C**) Production of ^{13}C (M+2) acetyl-CoA and ^{13}C (M+3) aspartate generated after a 1 hour pulse of 1mM 3-carbon labelled ^{13}C (M+3) pyruvate in ^{12}C pyruvate free media, expressed as a percentage of the total amount of detected metabolite, in primary hepatocytes from C57Bl/6J (white bars, n = 6) and *Tst*$^{-/-}$ (red bars, n = 5) normal diet-fed mice. (**D**) Blood glucose during the pre-clamp phase of the hyperinsulinemic, euglycemic clamp from C57Bl/6J (black lines), and *Tst*$^{-/-}$ (red lines) fed a control (ND, solid lines, n = 3, 6) or high fat diet (HFD, broken lines, n= 6, 7). (**E**) Mean integrated radioactive glucose (inversely related to whole body glucose uptake) during a hyperinsulinemic, euglycaemic clamp from normal diet fed C57Bl/6J control (white, n = 3), and *Tst*$^{-/-}$ (red, n = 6) mice. (**F**) Plasma glucose expressed as % of baseline glucose, over 120 minutes following insulin (i.p., 1mU/g) administration in 4 hour fasted C57Bl/6J (black line, n = 8) and *Tst*$^{-/-}$ (red line, n = 7) normal diet-fed mice. (**G**) HPLC quantified total and VLDL plasma triglyceride in 4 hour fasted C57Bl/6J (white bar, n = 6), and *Tst*$^{-/-}$ (red bar, n = 6) normal diet-fed mice. (**H**) Representative light microscopic images of fixed liver stained with Oil-Red O from normal diet-fed (ND) or high fat diet-fed (HFD) C57Bl/6J and *Tst*$^{-/-}$ mice. (**I**) Analysis of the area of red staining (Oil Red O) after thresholding, using Image J, from normal diet-fed (no pattern, n = 3-4/genotype) or high fat diet-fed (hatched pattern, n = 4-5/genotype) C57Bl/6J (white bars) and *Tst*$^{-/-}$ (red bars) mice. Data are represented as mean ±SEM. Significance was calculated using repeated measures ANOVA (**A**,**F**) 2-WAY ANOVA (**C**,**I**), 3-WAY repeated measures ANOVA (**D**) or unpaired two-tailed student's t-test (**B**,**E**,F,**G**) * $P < 0.05$, ** $P < 0.01$, *** $P < 0.001$, **** $P < 0.0001$. For (**C**) the 2-WAY ANOVA revealed no overall effect of genotype, however a significant interaction between metabolite and genotype was found. The * on the histogram represents this interaction. For (**D**) significant effects of time (****), diet (*) and genotype (*) were found. For (**F**) the analysis was performed on absolute glucose values and demonstrated a significant effect of time (****) and an interaction between time and genotype (*). T-tests revealed that the decrement of glucose from baseline at 30 and 60 minutes after insulin was greater in the *Tst*$^{-/-}$ (*). For (**I**) no main genotype effect was found, but a significant effect of diet (***), and an interaction (*) were found. Post Hoc analysis using Sidaks' multiple comparison test show an effect of diet on the 6J controls (***), whereas no effect of diet is found on the *Tst*$^{-/-}$.

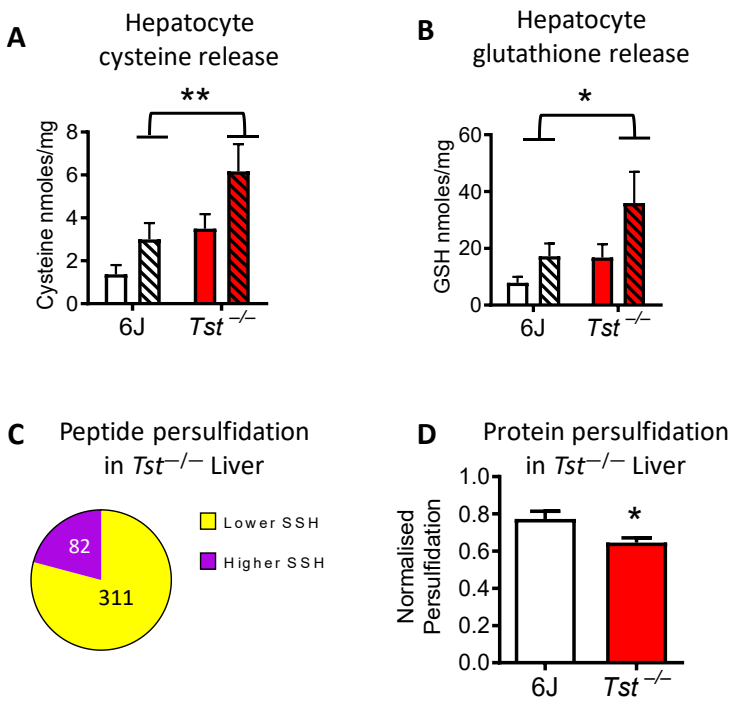

Figure 2. *Tst* deletion results in increased hepatic sulfur excretion and a reduction of protein persulfidation. (**A**) Cysteine concentrations (MBB-HPLC) in the media incubated with primary hepatocytes in the presence (hatched pattern) or absence (no pattern) of 1mM methionine, from C57Bl/6J (white bars, n = 4/treatment) and *Tst*$^{-/-}$ (red bars, n = 4/treatment) mice. (**B**) Glutathione concentrations (MBB-HPLC) in the media incubated with primary hepatocytes in the presence (hatched pattern) or absence (no pattern) of 1mM methionine, from C57Bl/6J (white bars, n = 4/treatment) and *Tst*$^{-/-}$ (red bars, n = 4/treatment) mice. (**C**) Pie chart depicting the proportion of liver peptides that are significantly higher (82 peptides, purple space) or lower (311 peptides, yellow space), in their persulfidation rate in the *Tst*$^{-/-}$ (n = 3) relative to C57Bl/6J (n = 3) mice. (**D**) Total DTT-released cysteine-persulfidated liver protein as measured by REVERT total protein stain following western blotting, normalised to the total input protein of the sample from *Tst*$^{-/-}$ (red bar, n = 4) and C57Bl/6J (white bar, n = 4) mice. Data with error bars are represented as mean ±SEM. Significance was calculated using 2-WAY ANOVA (**A**, **B**) or student's t-test (**D**), * $P < 0.05$, ** $P < 0.01$. For (**A**) and (**B**) the 2-WAY ANOVA reveals a main effect of genotype, indicated by * or ** on the histogram. A significant effect of methionine was also found for both (**A**) and (**B**) not indicated on the histogram. For (**C**) peptides were selected as being significant at a P-diff of 0.95 or greater.

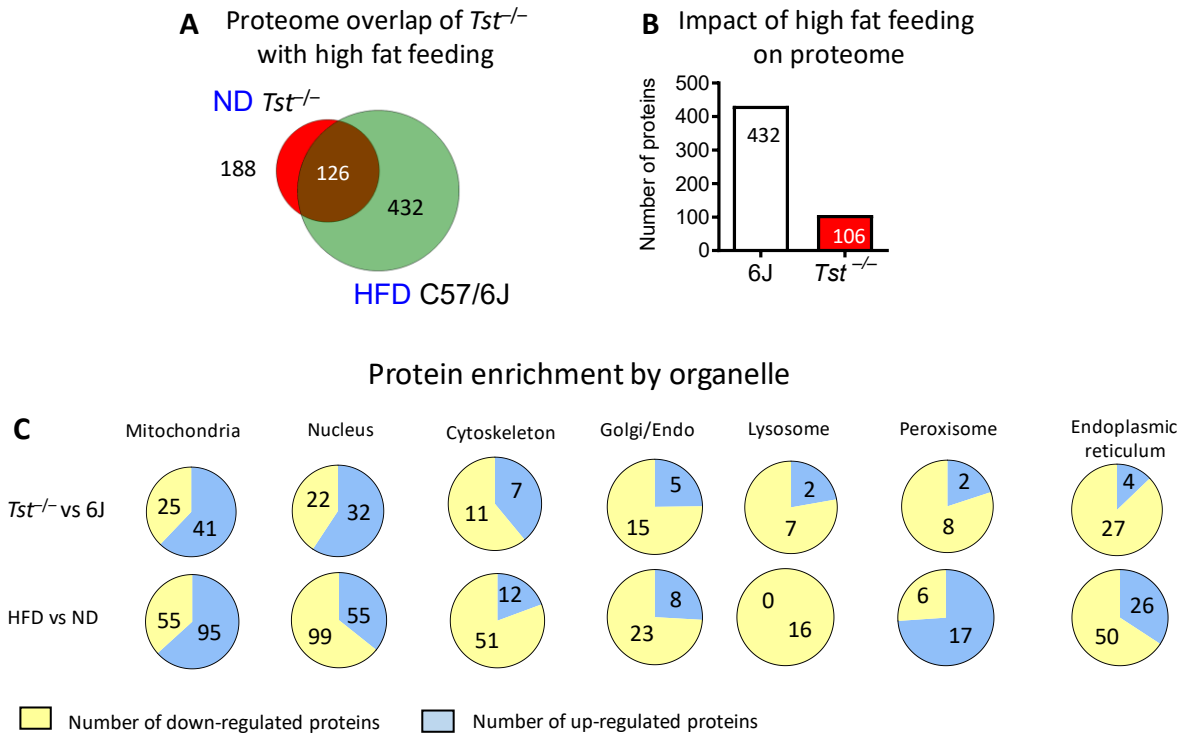

Figure 3. *Tst* deletion engenders a high fat feeding–like hepatic proteome with a distinct organellar signature. (**A**) Venn diagram representing the number of proteins significantly different (at P < 0.01) between normal diet-fed *Tst*$^{-/-}$ and C57Bl/6J (Red circle), and the number of regulated proteins between high fat fed and normal diet-fed C57Bl/6J (Green circle). The overlap (brown) represents those proteins regulated in the same direction by both comparisons (n= 4/genotype). (**B**) Number of proteins significantly different (at p < 0.01) between 58% high fat and normal diet in either C57Bl/6J (white bar), or *Tst*$^{-/-}$ mice (Red bar), (n= 4/genotype). (**C**) Pie charts depicting the proportion of individual liver proteins that are upregulated (Blue space) compared to downregulated (yellow space) after GO term categorisation according to subcellular location. Upper row; normal diet-fed *Tst*$^{-/-}$ relative to normal diet-fed C57Bl/6J. Lower row, high fat-fed C57Bl/6J relative to normal diet-fed C57Bl/6J.

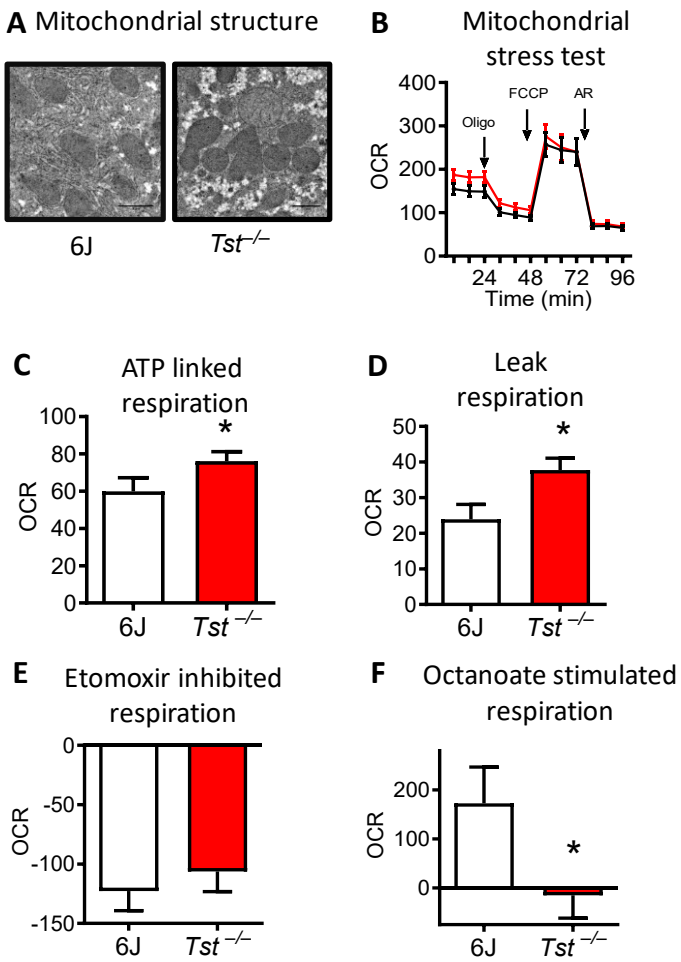

Figure 4. *Tst* deletion results in increased hepatocyte respiration but impaired medium–chain fat respiration. (**A**) Electron microscope images of liver, visualising mitochondria from normal diet-fed C57Bl/6J (n = 4) or *Tst*$^{-/-}$ (n = 4) mice. (**B**) Seahorse trace representing the mean oxygen consumption rate (OCR), normalised to protein, by hepatocytes from normal diet-fed C57Bl/6J (n = 6) or *Tst*$^{-/-}$ (n = 6) mice during a mitochondrial stress test. (**C**) Respiratory OCR linked to ATP production (oligomycin sensitive) by hepatocytes from normal diet-fed C57Bl/6J (n = 6) or *Tst*$^{-/-}$ (n = 6) mice, calculated from Figure 4B. (**D**) Respiratory OCR relating to proton leak (oligomycin insensitive) by hepatocytes from normal diet-fed C57Bl/6J (n = 6) or *Tst*$^{-/-}$ (n = 6) mice, calculated from Figure 4B. (**E**) Reduction of maximal uncoupled respiration following inhibition of long chain fatty acid mitochondrial import using etomoxir (8 µM), from normal diet-fed C57Bl/6J (n = 4) or *Tst*$^{-/-}$ (n = 4) mice. (**F**) Stimulation of maximal uncoupled respiration following addition of medium chain fatty acid octanoate (250 µM), from normal diet-fed C57Bl/6J (n = 4) or *Tst*$^{-/-}$ (n = 4) mice. Data are represented as mean ±SEM. Significance was calculated using an unpaired two tailed, student's t-test (**C**, **D**, **E**, **F**), * $P < 0.05$.